Velocity measurements of the laminar flow through a rotating straight pipe

U. Lei,[a] M. J. Lin, H. J. Sheen, and C. M. Lin
Institute of Applied Mechanics, National Taiwan University, Taipei 106, Taiwan, Republic of China

(Received 19 October 1993; accepted 22 February 1994)

Some measurements have been obtained for the axial velocity of the fully developed laminar flow in a circular straight pipe with radius a, which is rotating with constant angular speed Ω about an axis perpendicular to its own axis. A diode laser LDA system was mounted together with a circulating pipe flow system on a rotating table for the experiment. According to previous analyses and calculations, there exist four types of axial velocity distributions that result from the various effects of the secondary flow on the main stream via the convection and Coriolis effect for different values of $R(=w'_m a/\nu)$ and $R_\Omega(=\Omega a^2/\nu)$, where w'_m is the mean axial velocity and ν is the kinematic viscosity of the fluid. The present study provides experimental validation for the previous theoretical and numerical analyses. Experiments have also been carried out for studying the asymptotic nature of the slow flow in a rapidly rotating pipe ($R_\Omega \gg 1$ and $R_\Omega \gg R$) and the rapid flow in a slowly rotating pipe ($RR_\Omega \gg 1$ and $R \gg R_\Omega$).

I. INTRODUCTION

Consider a fluid flowing through a rotating circular straight pipe with radius a in Fig. 1. Let (r',θ,z') be the rotating right-handed cylindrical coordinates moving with the pipe wall and (u',v',w') be their corresponding velocity components. Also, let (x',y',z') be the Cartesian coordinates corresponding to (r',θ,z'). The pipe is rotating with a constant angular velocity $-\Omega\hat{j}$, where $\hat{j}$ is the unit vector along the y' axis. The axial primary flow, starting from negative z' to positive z', is maintained by an imposed axial pressure gradient. The secondary flow is set up in the $r'\theta$ plane by the Coriolis force through its interaction with the viscous force and the pressure gradients in the r' and θ directions. The flow is symmetric about the plane $y'=0$. In the present study, we restrict ourselves to the laminar fully developed cases with gravity $\mathbf{g}$ in the y' direction. The flow field is characterized by two independent dimensionless parameters: R_Ω and R, where $R_\Omega(=\Omega a^2/\nu)$ is the rotational Reynolds number and $R(=w'_m a/\nu)$ is the Reynolds number. Here ν is the kinematic viscosity of the fluid and w'_m is the axial mean velocity. Other dimensionless groups of interests, including those employed by the previous investigators, can be derived from R_Ω and R.

The problem for the fully developed laminar flow has been studied quite extensively via analytical methods and numerical calculations, which include the perturbation analyses by Baura,[1] Benton,[2] Berman and Mockros,[3] and Mansour,[4] the boundary layer analyses by Benton and Boyer[5] and Ito and Nanbu,[6] and the numerical calculations by Duck[7] and Lei and Hsu.[8] Among these studies, Berman and Mockros[3] obtained a third-order regular perturbation solution for small parameter N_α ($=R_\Omega/48$ here) for flow in a rotating nonaligned straight pipe. Their solution includes cases when the rotation axis makes an angle $\alpha(0\leqslant\alpha\leqslant 90°)$ with the pipe axis, and is expressed in terms of two-dimensionless parameters: $N_\alpha^2(=R_\Omega^2/2304$ here) and $N_R N_\alpha$ ($=R_\Omega R/24$ here). They found that there exists four types of flow regimes as follows. (1) Regime A: the flow is essentially axisymmetric and is similar to that of the Poiseuille solution when both $N_R N_\alpha$ and N_α^2 are small. (2) Regime B: In the regime where N_α^2 is small but $N_R N_\alpha$ is not, the effect of rotation is to skew the parabolic axial velocity profile (Hagen–Poiseuille) toward the outside, i.e., rotation moves the location of maximum axial velocity outward along $\theta=0°$ in Fig. 1. (3) Regime C: In the regime where $N_R N_\alpha$ is small but N_α^2 is not, the effect of rotation is to reduce the centerline velocity and produce an axial velocity profile with two maxima, one along $\theta=90°$ and one along $\theta=270°$. (4) Regime D: If both $N_R N_\alpha$ and N_α^2 are of significant size, the axial velocity profile is skewed with two maxima, which occur symmetrically in the first $(0°<\theta<90°)$ and the fourth $(270°<\theta<360°)$ quadrants in Fig. 1. These four flow regimes were confirmed and extended by Lei and Hsu's[3] calculation for the perpendicular rotating case ($\alpha=90°$). Through a series of scaling analyses and a detailed calculation, Lei and Hsu were able to classified quantitatively the parameter regimes for the above four flow regimes. The boundary layer analysis by Benton and Boyer[5] belongs to regime C and that by Ito and Nanbu[6] belongs to regime B. Regime D is the intermediate region between regime B and C. The relative positions in the parameter space for these four flow regimes are sketched in Fig. 2 in terms of the present parameters (R_Ω and $R_\Omega R$) according to Lei and Hsu.[8] The regions studied analytically by Berman and Mockros,[3] Benton and Boyer,[5] and Ito and Nanbu[6] are shown in Fig. 2. The region studied numerically by Lei and Hsu[8] bridges the above three "analytical" regions, and cover the whole region studied by Berman and Mockros. Also shown in Fig. 2 are the typical normalized axial velocity contours in the $r'\theta$ plane for these four flow regimes. Recall that the flow is symmetric about the plane $y'=0$ in Fig. 1, and here only half of the $r\theta$ plane is shown in Fig. 2. The contour values starting from the semicircular boundary are $w'/w'_{\max}=0$, 0.2, 0.4, 0.6, 0.8, and 0.95, respectively, where $w'_{\max}$ is the maximum axial velocity. The location of $w'_{\max}$ is denoted by a circular dark point in each case. Typical three-dimensional sketches

[a]Author to whom correspondence should be addressed.

 1070-6631/94/6(6)/1972/11/$6.00

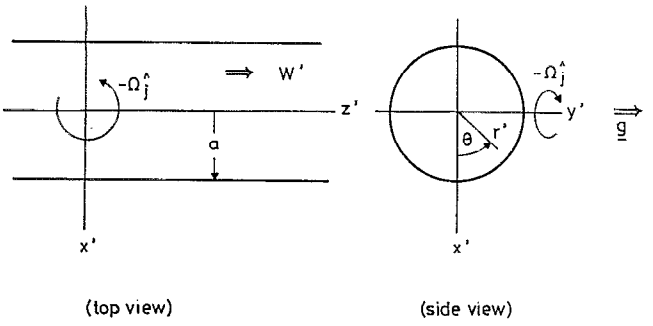

FIG. 1. The coordinates of the rotating pipe flow in the present study.

of the axial velocity profiles for the above four flow regimes can be found from Berman and Mockros.[3]

The previous experimental studies for this problem are rare in comparison with the analytical and numerical works. Benton and Boyer[5] obtained the axial velocities along the x' axis on the symmetric plane for ten cases ranging from R_Ω=1250−2778 with $R_c = w_0' a/\nu \approx 290 - 335$ (i.e., the regime C) by measuring the axial motion of the dye from photographs taken on a rotating table, where w_0' is the axial velocity on the pipe axis. They found that their measurements were in agreement with their analyses within 10% discrepancies for $-0.46<x'/a<0.46$. Ito and Nanbu[6] measured the reduced pressure drop at the fully developed region for wide ranges of R and R_Ω. They also measured a profile for the axial velocity distribution along the x' axis when R=2000 and R_Ω=250 (regime B) using a pitot tube mounted with the pipe system on a rotating mechanism.

Although the basic physics of the laminar fully developed pipe flow in a rotating frame is clearly understood through the previous studies mentioned above, a rigorous experimental validation for the four flow regimes is still lacking in the literature. The primary goal of this paper is thus to provide such validation by measuring the axial velocity for different parameters. This paper also aims to study the asymptotic nature of the slow flow in a rapidly rotating pipe

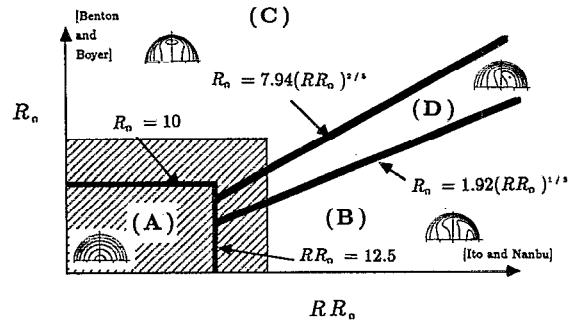

FIG. 2. The relative positions of the four flow regimes (A, B, C, and D) in the parameter diagram for the present rotating pipe flow together with the typical sketches of the axial velocity contours for different regimes. The shaped region was studied by Berman and Mockros. Also indicated in the diagram are the regions for the validity of the asymptotic results for the rapid flow in a slowly rotating pipe by Ito and Nanbu and the slow flow in a rapidly rotating pipe by Benton and Boyer.

(Benton and Boyer[5]) and the rapid flow in a slowly rotating pipe (Ito and Nanbu[6]). Besides, the calculations by Duck[7] are different from those by Lei and Hsu[8] for R_Ω=5 and R=430 −1107. The present study also provides an experimental investigation to those cases to see if there may exist dual solutions for such parameters. The results of the present study have engineering applications in the design of the cooling channels inside the rotating blades of gas turbines (see Morris[9]), and of some pipe flow systems in a rotating frame such as those on a spinning satellite.

II. EXPERIMENTAL DETAILS

As the flow occurs in a rotating frame, both the circulating pipe flow system and the devices for velocity measurements were mounted on a rotating table for the experiment. The rotating table, the measuring device and the circulating pipe flow system are sketched in Fig. 3, and are described as follows.

The rotating table was made of two circular disks with 80 cm in diameter and 2.3 cm in thickness. The upper disk was made of steel and the lower disk was made of cast iron, and both disks were mounted on a vertical hollow shaft with outside diameter 5 cm. The spacing between the two disks is 11 cm. The space between the two disks was employed to install the laser driver of the measuring device, the balancing masses for steady and stable rotation, the signal connection board and the electric power module. The rotating table was driven by a dc motor through a belt. The rotation speed could be varied from 0.005−1 rps (revolutions per second) by altering the input voltage of the dc motor, and was measured by recording the time spent in a given number of revolutions using a stop watch. The upper disk was drilled with holes such that the measuring device and the circulating pipe flow system could be mounted on it for the experiment. In order to transfer the measuring signals from the rotating frame to the outside inertial frame, a slip ring with 48 poles was installed at the bottom part of the shaft. The wires connecting the poles of the moving (inner) part of the slip ring and the signal connection board on the rotating table were placed and fixed inside the hollow shaft. The instruction signals could also be sent into the rotating frame from outside through the slip ring. There are up to 48 signals that can be transferred between the rotating and the inertial frame. The stationary (outer) part of the slip ring was connected to a signal connection board in the inertial frame, which was installed on the case of the rotating table. The case is a square box made of steel plates, which contains the bottom part of the shaft, slip rings, motor, belt, and wires. A slip ring for power supply was also installed on the shaft and connected to the electric power module between the two disks. Several transformers are included in the power module such that the power module can provide dc 5 V, dc 12 V, ac 100 V, and ac 110 V power sources to the devices installed on the rotating table.

The devices for velocity measurements include a forward scattering diode laser Doppler anemometer (LDA) system and a three-axis traversing table. The diode laser LDA system is a light weight, compact device in comparison with the traditional He–Ne and argon–ion laser LDA system. There are two parts of the present LDA system, the part

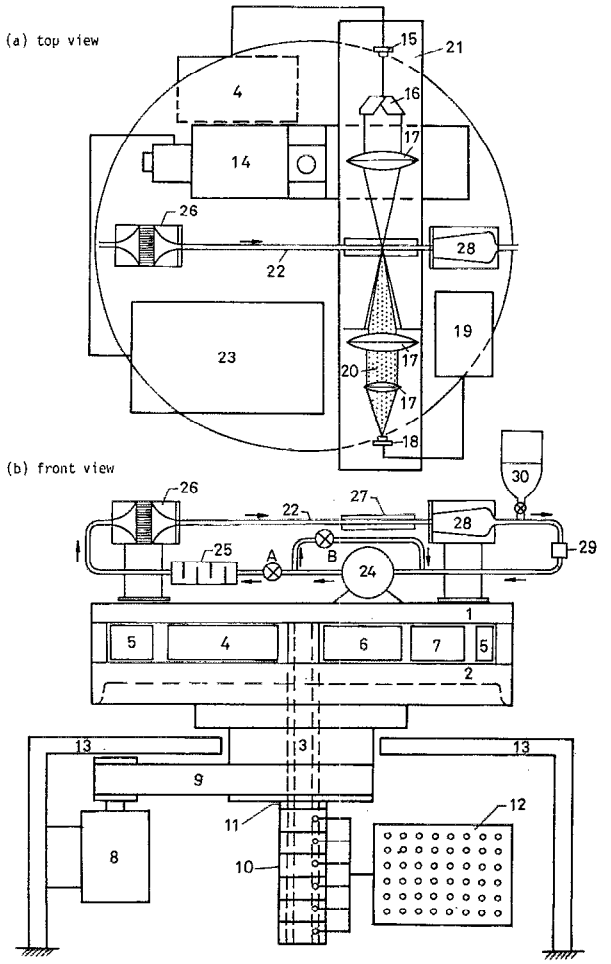

FIG. 3. Sketch of the apparatus of the present study. The components are (1) upper disk, (2) lower disk, (3) shaft, (4) laser driver, (5) balancing masses, (6) signal connection board on the rotating frame, (7) electric power module, (8) dc motor, (9) belt, (10) slip ring for transfering the signals, (11) slip ring for transferring the electric power, (12) signal connection board on the inertia frame, (13) case, (14) three-axis traversing table, (15) laser head, (16) beam splitter, (17) focus lenses, (18) avalanche photodiode (APD), (19) power supply for the APD receiver, (20) scattering light, (21) aluminum plate, (22) test section, (23) control box of the traversing table, (24) pump, (25) flow buffer, (26) honeycomb and flow contractor, (27) square box, (28) diffuser, (29) flow meter, and (30) reservoir.

installed on the rotating table [see Fig. 3(a)] and the signal processing part in the inertial frame. Consider first the part installed on the rotating table, which includes a laser driver, laser head, collimator, prism pair, beam splitter, three focus lenses, several ring mounts, and a APD (avalanche photodiode) receiver. The diode laser generates a 40 MW laser beam with wavelength 834 nm. The laser beam which is emitted from the laser head is separated into two parallel beams by the beam splitter. These two parallel beams are then focused through a focus lens to form a measuring volume. The Doppler signals are collected through two focus lenses, and are received by the APD receiver. The APD receiver includes a power supply and an avalanche photodiode with 150 Hz to 125 MHz bandwidth, 500–1000 nm spectral range and a 200 μm pinhole. The laser head, the lenses, and the avalanche photodiode were all fixed on an aluminum plate once they had been adjusted, and were mounted along the x' axis of the

TABLE I. The equation for the path traced out by the center of the measuring volume within $x^2+y^2\leq 1$ for (a) $m_g=1.52$ (quartz glass) and $m_S=1.452$ (85% glycerin–15% water solution), and (b) $m_g=1.52$ (quartz glass) and $m_w=1.33$ (water).

h	path with square box	path without square box
(a) $m_g=1.52$ and $m_S=1.452$		
0.1	$y=0.000\,349x+0.100$	$y=-0.0286x+0.0689$
0.2	$y=0.000\,726x+0.200$	$y=-0.0578x+0.138$
0.3	$y=0.001\,17x+0.300$	$y=-0.0882x+0.208$
0.4	$y=0.001\,73x+0.400$	$y=-0.121x+0.278$
0.5	$y=0.002\,50x+0.500$	$y=-0.156x+0.349$
0.6	$y=0.003\,67x+0.600$	$y=-0.196x+0.421$
0.7	$y=0.005\,66x+0.700$	$y=-0.244x+0.496$
0.8	$y=0.009\,72x+0.800$	$y=-0.303x+0.575$
0.9	$y=0.0212x+0.892$	$y=-0.385x+0.664$
(b) $m_g=1.52$ and $m_w=1.33$		
0.1	$y=0.000\,973x+0.100$	$y=-0.0223x+0.0752$
0.2	$y=0.002\,02x+0.200$	$y=-0.0450x+0.151$
0.3	$y=0.003\,23x+0.300$	$y=-0.0686x+0.226$
0.4	$y=0.004\,74x+0.400$	$y=-0.0939x+0.303$
0.5	$y=0.006\,77x+0.500$	$y=-0.122x+0.378$
0.6	$y=0.009\,73x+0.600$	$y=-0.153x+0.456$
0.7	$y=0.0145x+0.700$	$y=-0.190x+0.536$
0.8	$y=0.0237x+0.801$	$y=-0.237x+0.618$
0.9	$y=0.0464x+0.901$	$y=-0.301x+0.706$

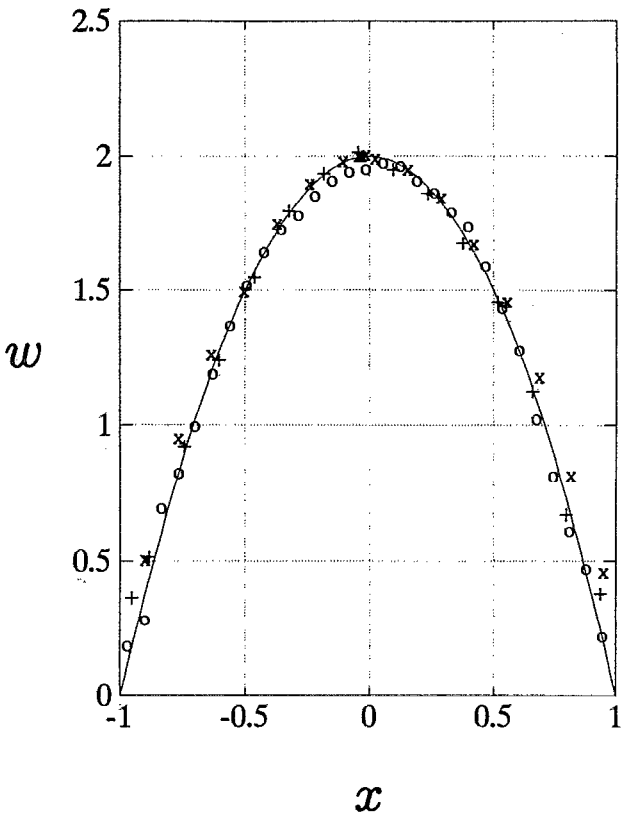

FIG. 4. The variations of the dimensionless axial velocity ($w = w'/w'_m$) with $x(=x'/a)$ in an inertial frame. The Poiseuille solution is represented by the curve. The present measurements are represented by the data points, O for $R=94.3$, + for $R=12.5$, and × for $R=457$.

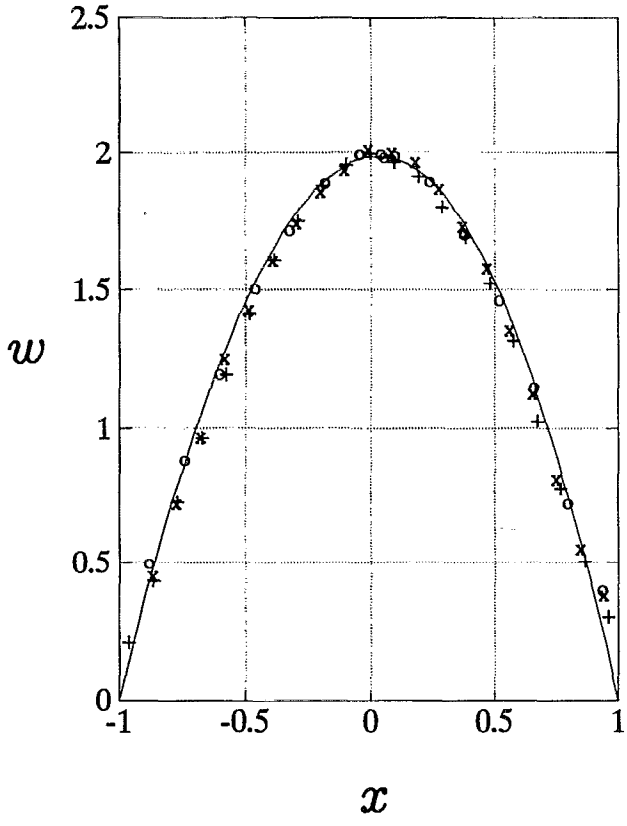

FIG. 5. Comparison of the dimensionless axial velocity distributions between the numerical solution by Lei and Hsu and the present measurements for different test sections and different downstream locations at $R=12.5$ and $R_\Omega=1$ (regime A). The numerical solution is represented by the curve. The measurements are represented by the data points, the circles (O) for $2a=1$ cm and $z'/a=90$, the plus symbols (+) for $2a=3$ cm, and $z'/a=28$, and the cross symbols (×) for $2a=3$ cm and $z'/a=21.8$.

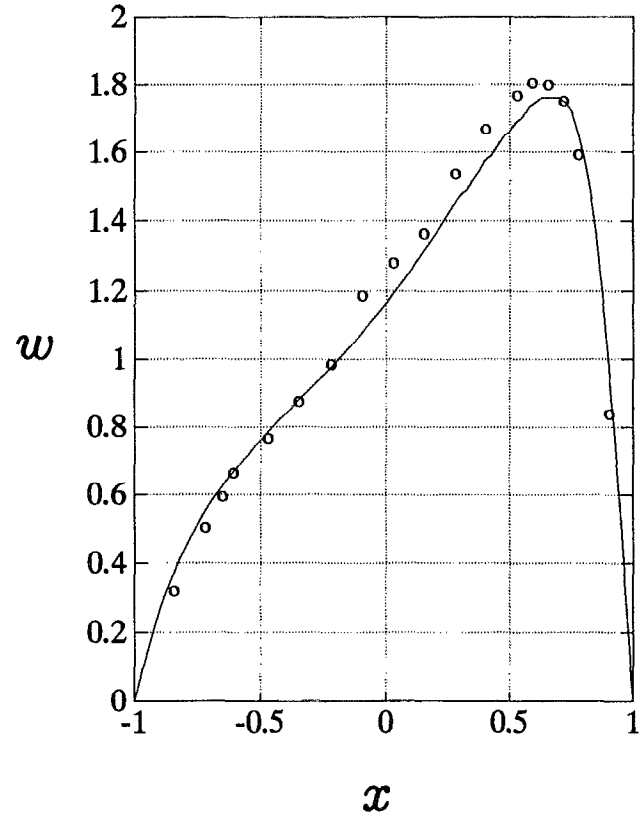

FIG. 6. Comparison of the dimensionless axial velocity distributions between the numerical solution by Lei and Hsu and the present measurement at $R=704$ and $R_\Omega=10$ (regime B). The numerical solution is represented by the curve, and the experimental results are represented by the circles.

three-axis traversing table. The directions of the axes of the traversing table are the same as those in Fig. 1, with the x' axis perpendicular to the axis of the test section discussed later in the circulating pipe flow system. As the laser light of the diode laser is invisible, an IR viewer was employed to adjust the laser beams and the measuring volume. The traversing table together with its control box were mounted on the upper disk of the rotating table. The motion of the traversing table (and hence, the measuring volume) was controlled by an 80286 personal computer in the inertial frame through the slip ring, and thus the measuring volume of the LDA system could be moved as desired while the rotating table was in motion. The power supply of the APD receiver was also mounted on the upper disk of the rotating table. The Doppler signals received by the avalanche photodiode were amplified by an amplified circuit built in the box of the power supply of the APD receiver, and then tranferred to the signal processing part of the LDA system in the inertial frame through the slip ring. The signal processing part includes a high-pass/low-pass filter, a digital burst correlator, an 80486 personal computer, and an oscilloscope. The Doppler signals went through the filter, the correlator and then the personal computer for data processing. The Doppler signals were monitored by using the oscilloscope during the experiment.

The circulating pipe flow system which was mounted on the upper disk of the rotating table is sketched in Fig. 3(b). It includes two loops: the primary loop for the main circulation and the secondary loop for the flow regulation. The fluid in the pipe flow system was pressurized by a pump. The fluid which left the pump first meets a T junction between the primary and the secondary loop. The flow rate of the primary loop and that of the secondary loop could be controlled by the valves A and B. When a large flow rate was required in the test section, valve B was closed such that the secondary loop was disabled. On the other hand, most of the fluid that left the pump would go through the secondary loop if a small steady low flow rate was required in the test section. Besides valves A and B, the flow rate could also be regulated by varying the input voltage of the ac motor which drove the pump. The fluid through the valve A would enter a flow buffer, which is a large hollow cylinder with alternating blocking plates in the flow direction. The primary role of the buffer was to trap the gas bubbles in the circulating pipe flow system, and the bubbles were removed through a ventilating valve located on the top of the buffer. In order to generate a "uniform" flow at the inlet of the test section, the fluid from the buffer was let to flow through a honeycomb and a smooth contractor before entering the test section. The test section is

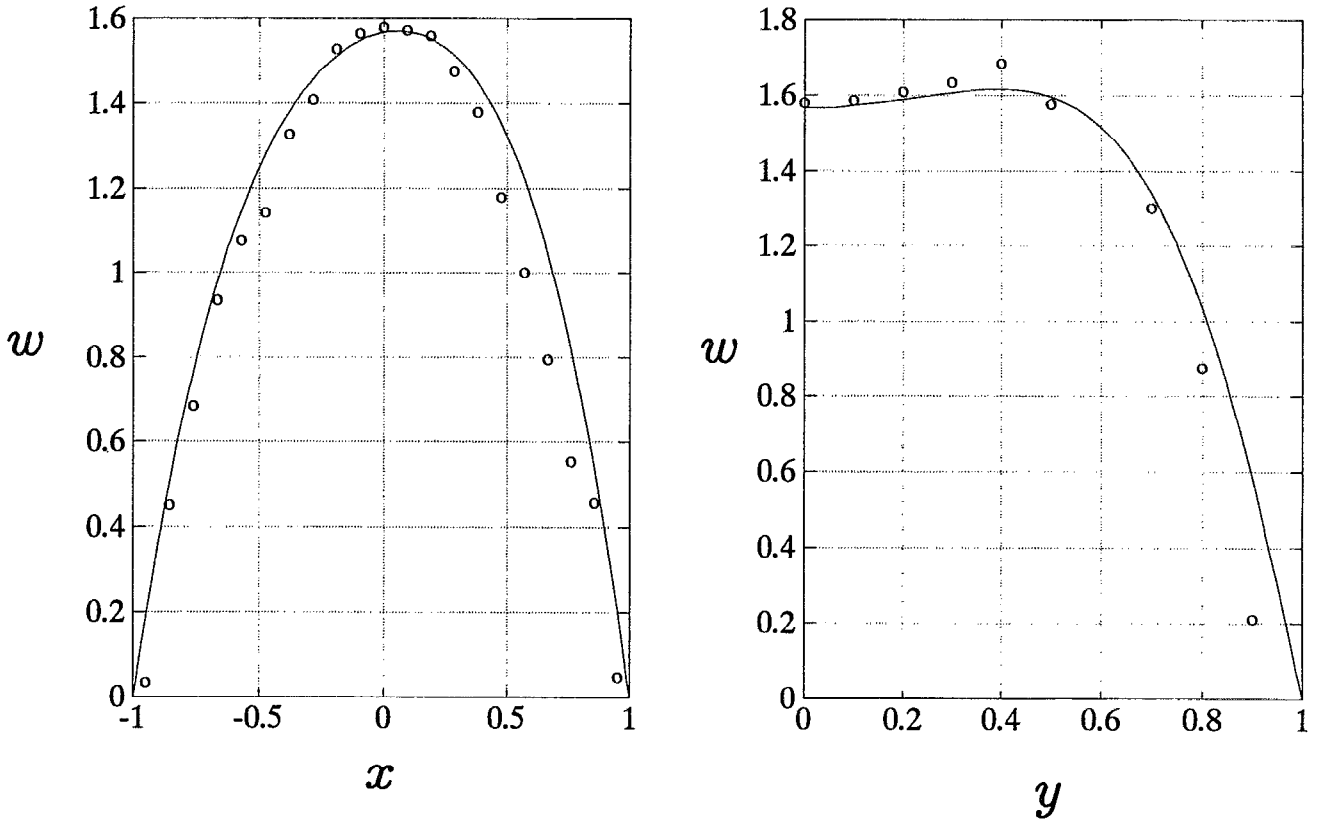

FIG. 7. Comparison between the numerical solutions by Lei and Hsu and the present measurements at $R=3.03$ and 17.4 (regime C). The numerical solutions are represented by the curves, and the measurements are represented by the circles.

a circular tube made with quartz glass, and the LDA measurements were taken at a downstream location sufficiently far from the inlet. For the laminar circular pipe flow in an inertial frame, the entrance length L_e, defined as the axial distance from the inlet required for the axial velocity on the pipe axis to reach 99% of the Poiseuille value, is

$$\frac{L_e}{2a} \approx \frac{0.6}{1+0.07R} + 0.112R, \tag{1}$$

according to Shah and London.[10] In case the pipe flow occurs in a rotating frame, L_e can be reduced substantially by the rotating effect, according to the calculation of the parabolized Navier–Stokes equations (Chen[11]) and the full Navier–Stokes equations (Yang[12]). The determination of whether the flow reaches the fully developed state for a given set of parameters was estimated by using the results of Shah and London,[10] Chen,[11] and Yang,[12] and by comparing the measurements at two neighboring axial locations. The two laser beams forming the measuring volume entered the test section along a plane with $y'=$const in Fig. 1. The path of the laser beam was deflected by the curvature of the tube except on the $y'=0$ plane, i.e., the horizontal movement of the traversing table along the x' axis (with y' and z' fixed) makes the center of the measuring volume inside the tube traces out a straight path with finite slope in the $x'y'$ plane except $y'=0$. In order to reduce the slope of the path of the measuring volume, a square box was built outside the circular tube, and the space between the tube and the wall of the box was filled with the same kind of fluid as that inside the test section. The two side walls perpendicular to the incoming laser beams were made of optical glass, and the other four sides of the square box were made of Plexiglas. Two holes were drilled on the upper wall of the square box for fluid filling and gas removement. The fluids employed in the present experiment were water and glycerin–water solution. The glycerin–water solution was seeded to enhance the laser scattering during the experiment. No seeding was required when the working fluid is water. Although the refractive indexes of the water (m_w) and the glycerin–water solution (m_S) are still slightly different from that of the quartz glass (m_g), the slope of the path traced out by the measuring volume is small after using the square box. Assume that the traversing table moves along the x' axis in a plane $y'=h'=$const. Let $x=x'/a$, $y=y'/a$ and $h=h'/a$. On using the principle of Fermat for refraction, the paths traced out by the center of the measuring volume inside the test section with or without the square box were evaluated and listed in Table I for $m_S=1.452$ (85% glycerlin–15% water), $m_w=1.33$, $m_g=1.52$, $a=1.5$ cm, and $t=0.125$ cm, where t is the thickness of the tube (the test section). It was found that the slope of the path is still very small even when $h=0.9$ for the case with square box. There were three types of test section employed for different parameters in the present experiments: (1) $2a=1$ cm and $L=60$ cm, (2) $2a=2$ cm and $L=120$ cm, and (3) $2a=3$ cm and $L=50$ cm, where L is the axial length of the test section. The fluid that left the test section went through a diffuser, an

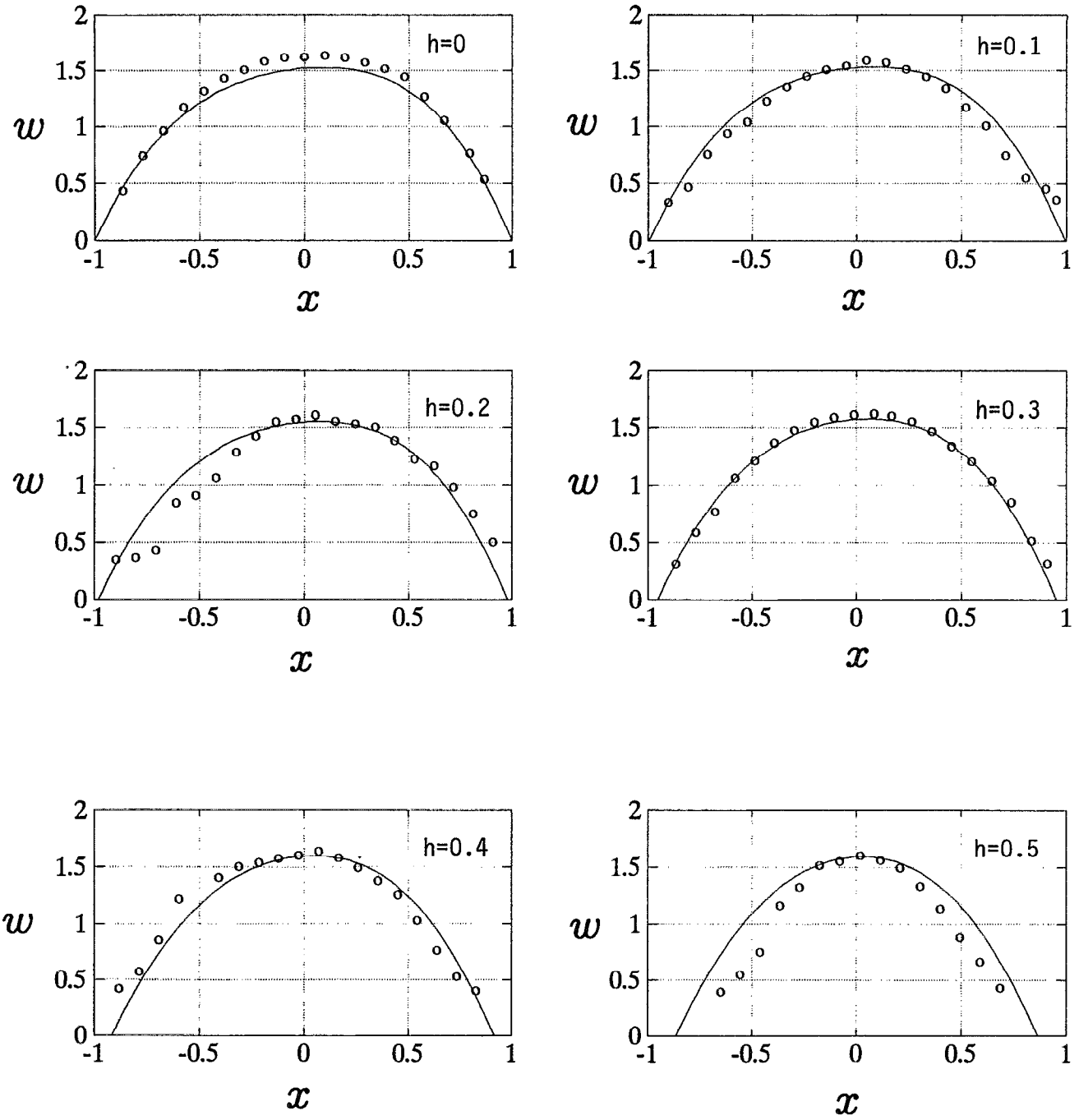

FIG. 8. Comparison of the dimensionless axial velocity distributions between the numerical solutions by Lei and Hsu and the present measurements at $R=4.73$ and $R_\Omega=20$ (regime D) at different values of h. The numerical solutions are represented by the curves, and the measurements are represented by the circles.

integrated-type flow meter and then entered the pump to complete a circulation loop. The output signal of the flow meter was sent outside from the rotating frame through the slip ring to a timer. A small reservoir with cover opening to the surrounding was also connected to the circulating system for filling the fluid and removing the gas. A thermometer could be inserted into the pipe flow system from the reservoir to measure the temperature of the flow.

There was no temperature control system in the present experiment. The whole system was let to run for a sufficiently long time (more than 30 min) such that the system was in thermal equilibrium before taking the data. The heat generated by the pump (a steady heat source of the circulating flow system) was removed by a fan installed on the rotating table, so that the temperature of the flow was limited to within 33 °C. The viscosities of the testing fluids at different temperatures were measured separately by using a digital viscometer together with a constant temperature bath. The viscosity of the fluid was determined once the temperature of the circulating system was measured. Thus for a given test

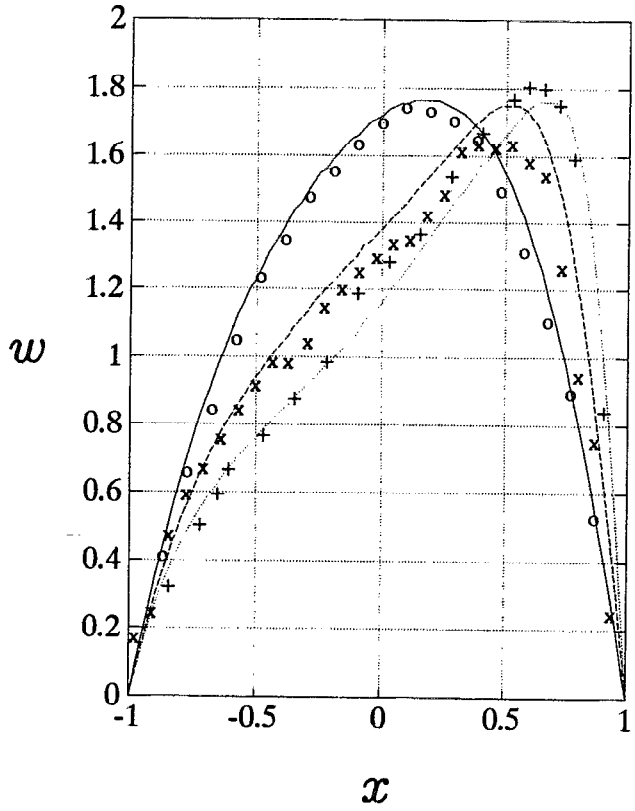

FIG. 9. The variations of the dimensionless axial velocity distributions for different values of R at $R_\Omega=10$. The numerical result by Lei and Hsu and the present experimental result are denoted by solid line and circles (O) for $R=10.9$, by dash line and cross symbols (×) for $R=94.3$, and by dotted line and plus symbols (+) for $R=704$, respectively.

section (given a), the two independent dimensionless parameters, R and R_Ω, for a given experiment were known after the volume flow rate (Q) and the rotation speed (Ω) were measured. The flow meter was calibrated before doing the experiment. Two methods of calibration were employed in the present study. For water, the flow meter was calibrated by measuring the volume of the fluid flow through the meter for a period of 100 s. The variations of the reading of the flow meter with the actual flow rate (Q) was linear up to $Q\approx100$ cm^3/s. As the viscosity of the glycerin–water solution varies significantly with temperature and moisture in the surrounding, the flow meter for cases with such fluid was calibrated by using the present circulating pipe flow system and the LDA system without turning the rotating table. For a given reading of the flow meter, the axial velocity at the pipe axis (w_0') in the laminar fully developed region was measured, which equals to $2w_m'$, according to the Poiseuille solution. The flow rate Q then equals to $\pi a^2 w_m'$. The latter calibration method using the pipe flow velocity measurement was also employed for water in order to ensure that both calibration methods give the same result. The data for the flow meter calibration can be found from Lin.[13] The effect of rotation on the reading of the flow meter was studied by varying the position of the flow meter on the rotating table (the flow meter is connected to the diffuser and the pump by soft tubes). It was found that the readings were essentially the same for different locations of the meter within the range of rotation speed for the present study. The alignment of the optics, the installation of the circulating pipe flow system and that of the LDA system were checked by comparing the measurements of the axial velocity profiles at different Reynolds number and $\Omega=0$ with the exact Poiseuille solution. The results for three different measurements along the x' axis with different Reynolds numbers are plotted in Fig. 4 together with the Poiseuille solution. The experiment with $R=457$ was carried out with water, and the remaining two measurements were carried out with glycerin–water solution. The experimental data are in good agreement with the exact solution.

III. RESULTS AND DISCUSSION

The four flow regimes mentioned above were validated by the following four cases: (1) $R=12.5$, $R_\Omega=1$ (regime A, Fig. 5); (2) $R=704$, $R_\Omega=10$ (regime B, Fig. 6); (3) $R=3.03$, $R_\Omega=17.4$ (regime C, Fig. 7); and (4) $R=4.73$, $R_\Omega=20$ (regime D, Fig. 8). The numerical solutions according to Lei and Hsu[8] for these four cases are also shown in Figs. 5–8. The test fluid for the experiment is water for case (B) and 85% glycerin–15% water solution for cases (1), (3), and (4). Let $w = w'/w_m'$, and recall that $x=x'/a$ and $y=y'/a$. Figure 5 shows three measurements for w along the x axis for case (1) at different downstream axial locations and with different test sections. It is found that the experimental results are essentially parabolic, and agree nicely with one another and with the numerical solution. The flow in regime B is characterized by a skewed axial velocity profile similar to that in curved pipe, with the maximum value occurs on the positive x axis. Figure 6 depicts the dimensionless axial velocity distribution (w) along the x axis for case (2), and there are good agreement between the experimental results and the numerical calculations. Figure 7 illustrates the dimensionless axial velocity distributions along the x axis and that along the y axis. Same as the numerical solutions, the experimental measurements indeed indicate that the axial velocity is essentially symmetric about the y axis and possesses a maximum at a positive y location. Note that the flow is symmetric about the symmetric plane $y=0$, and here only the result for $y\geqslant0$ is shown in Fig. 7(b). The symmetry of the flow field about $y=0$ had been checked experimentally, and the results can be found form Lin.[13] Figure 8 shows the axial velocity distributions along the x axis for different values of h (see Table I). Here h is the dimensionless distance of the laser beam from the symmetric plane $y=0$ outside the test section, which can be controlled and adjusted easily by the movement of the three-axis transversing table. The measurements in Fig. 8 are the axial velocities along straight lines with finite slopes in the xy plane, and thus two position variables are required for illustrating the measurements. Here we employed x and h. The equations of the straight lines where the measurements were taken are listed in Table I for different values of h. The measurements are in agreement with the calculations, and the axial velocity is skewed toward the pressure (positive x) side with the maxima occur slightly on the right of the y axis.

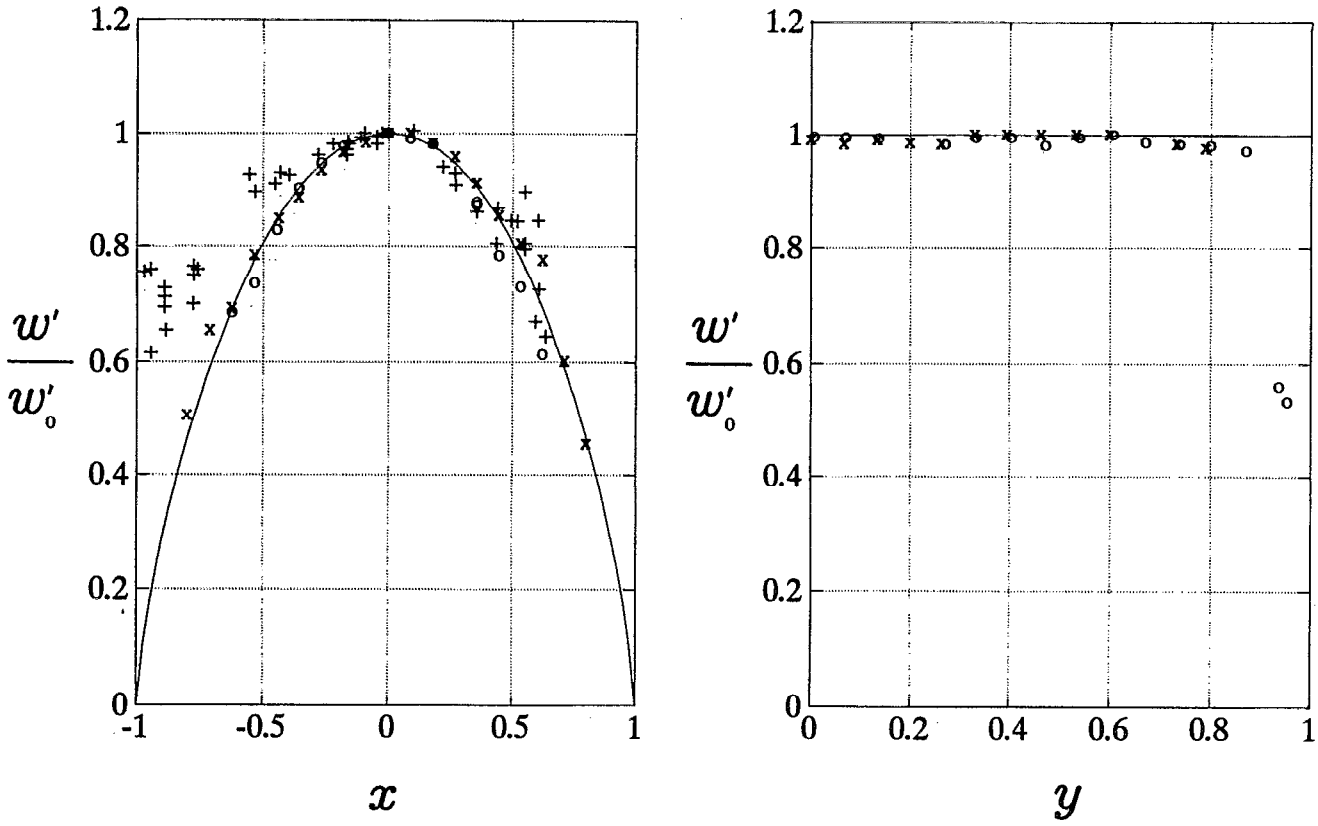

FIG. 10. Study of the asymptotic case for $R_\Omega \gg 1$ and $R_\Omega \gg R$. The asymptotic solutions by Benton and Boyer are represented by solid lines. The measurements by Benton and Boyer are represented by the plus symbols (+). The present measurements at $R_\Omega = 1250$ are represented by the circles (○) and the cross symbols (×) for $R = 250$ and $R = 452$, respectively.

As discussed in Lei and Hsu,[8] the different flows in the four different flow regimes are resulted from the various effects of the secondary flow on the main stream via the convection and the Coriolis mechanisms, and can be understood clearly through a scaling analysis of the equations governing the fluid motion. There are four terms in the axial momentum equation for the present fully developed pipe flow in the rotating frame in Fig. 1 (see Lei and Hsu[8]): the convection term due to the secondary flow, the pressure term which drives the flow, the Coriolis term and the viscous term. The flow is axisymmetric and possesses a maximum on the pipe axis when both the convection and the Coriolis effects are absent. The convection effect tends to move the location of the maximum axial velocity along the positive x axis, while the Coriolis effect tends to reduced the axial velocity near the center and produces a dumbell-like profile with two maxima located symmetrically on the positive and negative y axis, respectively. For regime A, both the convection and the Coriolis terms are negligible, the flow is thus essentially axisymmetric and similar to that of the Poiseuille solution. For regime B, the convection term is of the same order as the pressure and viscous terms, and pushes the location of the maximum axial velocity toward the pressure side (positive x). For regime C, the Coriolis term, the pressure term and the viscous terms are of equal importance, and thus the axial velocity shows a dumbell-like profile. All of the four terms are significant for the flow in regime D. Both the convection and the Coriolis mechanisms are acting on the flow, and thus the flow is skewed toward the pressure side with two maxima in regime D. The parameters for the results in Figs. 5–8 are selected such that they are located separately in the four different regimes in Fig. 2. As the magnitudes of the terms in the axial momentum equation depend continuously on the parameters R and R_Ω, the flow in one regime transits smoothly to the other regime as the parameters vary. Figure 9 shows that the maximum value of the axial velocity profile shifts continuously toward the pressure side as R increases (the convection effect increases) for $R_\Omega = 10$, and the measurements agree nicely with the calculations. Other results of the variations of the flow as the parameters vary may be found from Figs. 10–12. Since the calculations by Lei and Hsu[8] were validated experimentally by the results in Figs. 5–9 and some other results in Lin,[13] detailed variations of the flow (including both the axial velocity and the secondary stream function) with the parameters can be found from Lei and Hsu. A scaling analysis for illustrating the essential physics of the flow phenomena can also be found from Lei and Hsu.

After the validation of the existence of the four flow regimes, we study the asymptotic case for slow flow in a rapidly rotating pipe when $R_\Omega \gg 1$ and $R_\Omega \gg R$, i.e., the limiting case for regime C. Benton and Boyer[5] proposed that the flow field can be analyzed by separating it into two regions: the core region and the boundary layer. The inertia force is

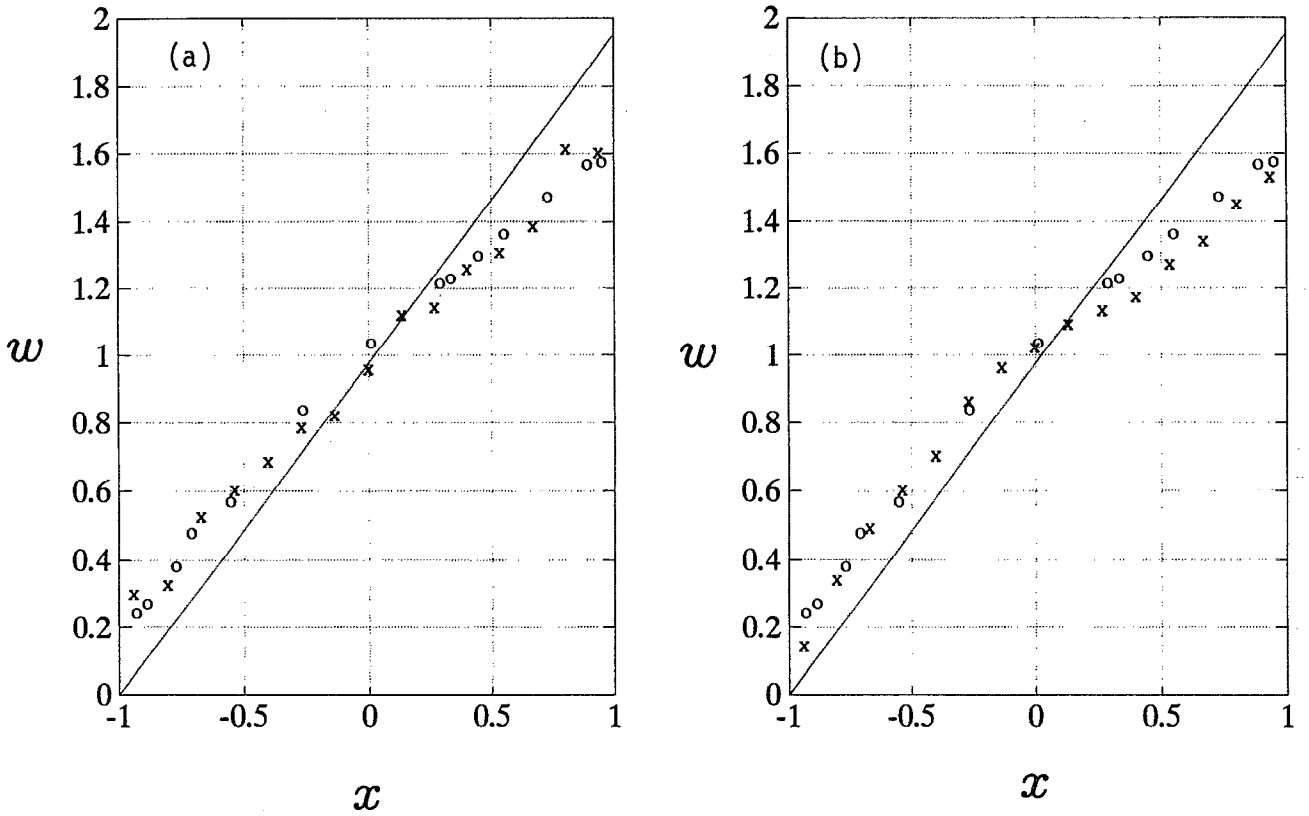

FIG. 11. Study of the asymptotic case for $R_\Omega \ll R$ and $RR_\Omega \gg 1$. The asymptotic solution by Ito and Nanbu is represented by the solid straight line. The experimental results for $R=2000$ and $R_\Omega=250$ by Ito and Nanbu are represented by the circles (○). The cross symbols (×) in (a) are the present measurements for $R=2000$ and $R_\Omega=250$ ($K_l=4\times10^6$ and $\Delta=0.125$), and that in (b) are the present measurements for $R=2500$ and $R_\Omega=250$ ($K_l=5\times10^6$ and $\Delta=0.1$).

not significant in either region. The thickness of the boundary layer is of order $a/R_\Omega^{1/2}$. The core region is geostrophic with the axial velocity distribution satisfying

$$w'/w_0'=(1-x^2)^{3/4}, \tag{2}$$

according to Benton and Boyer, where w_0' is the axial velocity along the pipe axis and is the maximum value in the asymptotic analysis. Note that w' is independent of y, according to Eq. (2). The calculations by Lei and Hsu[8] show that Eq. (2) is valid for $R_\Omega/R \geqslant O(10)$ and $|y| \leqslant 0.5$ when $R_\Omega=100$. However, the maximum values of w' occur at $r'/a=0.75$ and $\theta=\pm90°$ instead of at $r'=0$ due to the various effects of the Coriolis force on the boundary layer flow at different azimuthal locations, which was explained by Lei and Hsu through a scaling analysis and is in qualitative agreement with the perturbation analysis by Berman and Mockros.[3] Benton and Boyer[5] verified their analytical result in Eq. (2) by carrying out a series of measurements of the axial velocity distributions on the symmetric plane ranging from $R_\Omega=1250-2778$ and $R_c \approx 290-335$ as mentioned in Sec. I. Note that R_c is greater than R. Due to the limitation of their measuring technique at that time, Benton and Boyer found that their measurements agree with their analysis within 10% error for $-0.46 \leqslant x \leqslant 0.46$. Figure 10 shows the present measurements of the axial velocity distributions along the x and the y axis together with the asymptotic solution [Eq. (2)] and the experimental results by Benton and Boyer. The parameters for the present measurements are $R_\Omega=1250$ and $R=250$ and 452. The present measurements are in good agreement with the asymptotic solution. It is found that the asymptotic solution for $R_\Omega \gg 1$ and $R_\Omega \gg R$ by Benton and Boyer is valid for $|y| \leqslant 0.85$ when $R_\Omega/R>3$ and $R_\Omega=O(10^3)$, which is a larger region for y in comparison with that for $R_\Omega=O(10^2)$ (see Lei and Hsu[8]) as expected. Also the lower limit of the validity of the asymptotic result for R_Ω/R is reduced as R_Ω increases by comparing the present experimental results with the calculations by Lei and Hsu.

For the rapid flow in a slowly rotating pipe when $K_l=8RR_\Omega \gg 1$ and $\Delta=R_\Omega/R \ll 1$ (i.e., the limiting case for regime B), Ito and Nanbu[6] proposed that the flow can be solved by separating it into two regions: (1) a thin boundary layer with thickness of order $aK_l^{1/4}$ near the wall of the pipe and (2) a frictionless core where the flow is influenced by inertia and pressure forces. They found that the axial velocity is linear with x in the core, and provided a set of experimental data for $R=2000$ and $R_\Omega=250$ (i.e., $K_l=4\times10^6$ and $\Delta=0.125$) to support their theory. The measurements agree fairly with the theory, as shown in Fig. 11(a). Also shown in Fig. 11(a) is the present experimental results with the same parameters as those in Ito and Nanbu. The present experimental result agrees nicely with the measurement by Ito and Nanbu. As the present measurement technique is different from that in Ito and Nanbu, the discrepancy between the

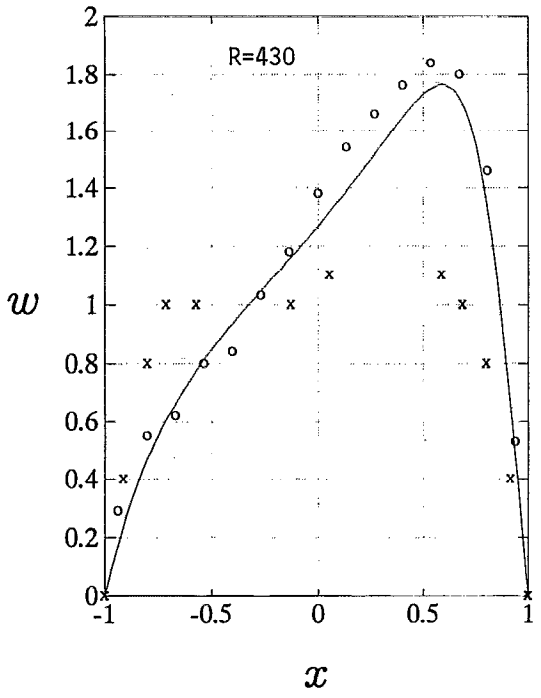

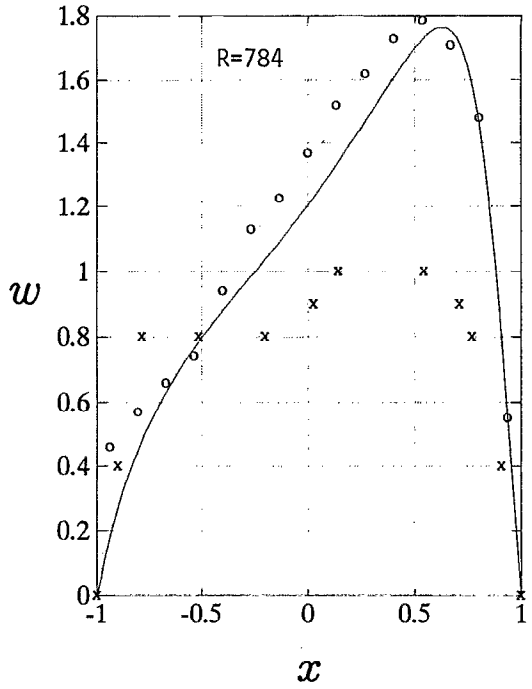

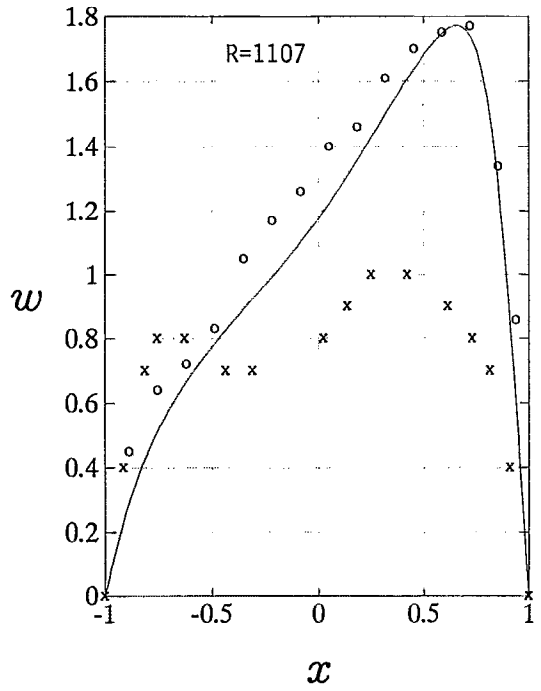

FIG. 12. Comparison of the dimensionless axial velocity between the present measurements (O), the numerical solutions by Lei and Hsu (curves), and the numerical solutions by Duck (×) at $R_\Omega=5$ and different values of R.

asymptotic theory and the experiments is not primary due to the accuracy of the measurements. In order to see if there may exist better agreement between the asymptotic theory and the experiments as either K_l increases or Δ decreases, we have carried out four additional measurements with K_l ranging from 3×10^6 to 5×10^6, and Δ ranging from 0.1 to 0.167. Note that for laminar flow, there exist an upper bound for K_l for a given value of Δ, since the flow may become unstable if K_l exceeds a critical value (see Ito and Nanbu[6]). The discrepancies among the four additional measurements and the experimental results in Fig. 11(a) are within experimental uncertainties. A typical result for $K_l=5\times10^6$ and $\Delta=0.1$ ($R=2500$ and $R_\Omega=250$) is plotted in Fig. 11(b) together with the asymptotic and the experimental results by Ito and Nanbu. It is found that the two experimental measurements in Fig. 11(b) with different parameters give almost the same result. Therefore, the "slightly" disagreement between the asymptotic solution and the experimental measurement is

probably due to the inherent nature of the assumptions in the asymptotic analysis. As convection is important in the core, the discrepancies between the asymptotic and the experimental results in Fig. 11 are assumed to be mainly due to the detrainment of the fluid from the boundary layer at $x=-1$ and the entrainment of the fluid into the boundary layer at $x=1$.

Although the dimensionless volume flow rate calculated by Duck[7] agrees fairly with that by Lei and Hsu[8] for the same values of R_Ω and R, the detailed flow field between these two calculations are significantly different from each other for $R_\Omega=5$ and $R=430$, 784, and 1107, as discussed in Lei and Hsu. The flow for such cases belong to regime B, which is similar to the flow in a loosely coiled pipe. As there may exist dual solutions in the curved pipe flow for large Dean number (see Dennis and Ng[14]), it is not certain that whether the difference between the calculations by Duck and that by Lei and Hsu is the consequence of the existence of dual solutions. Figure 12 shows the measurements of the axial velocity distributions along the x axis for the above three cases together with the numerical results by Duck[7] and by Lei and Hsu.[8] The results by Duck were obtained from their axial velocity contours. It is found that the experimental results agree with the solutions by Lei and Hsu. In order to check if the "disturbances" of the system can affect the experimental results in Fig. 12, we first adjusted the rotating table to the speed corresponding to $R_\Omega=5$, and then adjusted R to the given value in two ways. One was to increase the pumping power (i.e., the volume flow rate) from zero, and the other was to decrease the volume flow rate from an initial large value. Both measurements gave essentially the same results.

Most of the experimental results shown in this paper were repeated twice. There are several resources of experimental uncertainties for the present measurements. The uncertainty associated with the diode laser, the optics and the electronics was estimated to be about 2% for the velocity measurement sufficiently far from the wall. Such uncertainty is larger for the measurement near the wall due to the velocity bias, and has been corrected during data reduction. The uncertainty for the near-wall measurement was then estimated to be about 6%. The uncertainty for the rotation speed was about 1%. The uncertainty for the volume flow rate was about 2%. The uncertainty for the viscosity (mainly due to the temperature variation) was about 3%. The uncertainty associated with the orthogonality between the laser beam and the side wall of the square box for the test section was estimated to be 4% for region not near the wall. Such uncertainty could be large for large y for the flow in regime C (as indicated by Figs. 7 and 10), since the location of the measuring volume which is expected to be located in the core, according to Table I, may fall actually inside the boundary layer.

IV. CONCLUSION

In this study, an experimental system was set up for studying the pipe flows in a rotating frame, which includes a rotating table, a circulating pipe flow system, and a diode laser LDA system together with a three-axis traversing table. The existence of the four flow regimes has been validated experimentally by measuring the axial velocity distributions for different parameters. Detailed variations of the flow with parameters and the essentially physics of the flow phenomena according to the previous analyses and calculations can then be accepted and employed with confidence. The asymptotic nature were also studied experimentally for the slow flow in a rapidly rotating pipe ($R_\Omega \gg 1$ and $R_\Omega \gg R$) by Benton and Boyer and for the rapid flow in a slowly rotating pipe ($RR_\Omega \gg 1$ and $R \gg R_\Omega$) by Ito and Nanbu. It is found that the asymptotic result by Benton and Boyer is valid when $R_\Omega/R>3$ for $R_\Omega=O(10^3)$. However, the agreement between the asymptotic result by Ito and Nanbu with the experiment is fair due to the inherent nature of the assumption made in the analysis. A preliminary investigation on the dual solution problem for small R_Ω and large R had also been carried out, and it was found that the solution is unique up to $R=1107$ for $R_\Omega=5$. The experimental system in the present study can be modified to study the entry flow and the turbulent flow in a rotating straight pipe. The work for the entry flow is in progress.

[1] S. N. Baura, "Secondary flow in a rotating straight pipe," Proc. R. Soc. London Ser. A **227**, 133 (1954).
[2] G. S. Benton, "The effect of the Earth's rotation on laminar flow in pipes," Trans. ASME: J. Appl. Mech. **23**, 123 (1956).
[3] J. Berman and L. F. Mockros, "Flow in a rotating non-aligned straight pipe," J. Fluid Mech. **144**, 297 (1984).
[4] K. Mansour, "Laminar flow through a slowly rotating straight pipe," J. Fluid Mech. **150**, 1 (1985).
[5] G. S. Benton and D. Boyer, "Flow through a rapidly rotating conduit," J. Fluid Mech. **26**, 69 (1966).
[6] H. Ito and K. Nanbu, "Flow in rotating straight pipes of circular cross section," Trans. ASME: J. Basic Eng. **93**, 383 (1971).
[7] P. W. Duck, "Flow through rotating straight pipes of a circular cross section," Phys. Fluids **26**, 614 (1983).
[8] U. Lei and C. H. Hsu, "Flow through rotating straight pipes," Phys. Fluids A **2**, 63 (1990).
[9] W. D. Morris, *Heat Transfer and Fluid Flow in Rotating Coolant Channels* (Wiley, New York, 1981), Chap. 6.
[10] R. K. Shah and A. L. London, *Laminar Flow Forced Convection in Ducts* (Academic, New York, 1978).
[11] R. H. Chen, "Calculations of the entry flow through a rotating straight pipe," Master thesis, National Taiwan University, 1989.
[12] C. Y. Yang, "Calculations of the fluid flow and heat transfer in a rotating straight pipe," Master thesis, National Taiwan University, 1990.
[13] M. R. Lin, "Experiments on the flow through a rotating straight pipe," Master thesis, National Taiwan University, 1992.
[14] S. C. R. Dennis and M. Ng, "Dual solutions for steady laminar flow through a curved tube," Q. J. Mech. Appl. Math. **35**, 305 (1982).